Solvent-mediated charge redistribution in photodissociation of IBr⁻ and IBr⁻(CO₂)

Leonid Sheps,[1,a)] Elisa M. Miller,[1] Samantha Horvath,[2,b)] Matthew A. Thompson,[1,c)] Robert Parson,[1,d)] Anne B. McCoy,[2,d)] and W. Carl Lineberger[1,d)]

[1]*JILA, Department of Chemistry and Biochemistry, University of Colorado, Boulder, Colorado 80309, USA*
[2]*Department of Chemistry, The Ohio State University, Columbus, Ohio 43210, USA*

A combined experimental and theoretical investigation of photodissociation dynamics of IBr⁻ and IBr⁻(CO₂) on the B ($^2\Sigma_{1/2}^+$) excited electronic state is presented. Time-resolved photoelectron spectroscopy reveals that in bare IBr⁻ prompt dissociation forms exclusively I* + Br⁻. Compared to earlier dissociation studies of IBr⁻ excited to the A' ($^2\Pi_{1/2}$) state, the signal rise is delayed by 200 ± 20 fs. In the case of IBr⁻(CO₂), the product distribution shows the existence of a second major ($\sim$40%) dissociation pathway, Br* + I⁻. In contrast to the primary product channel, the signal rise associated with this pathway shows only a 50 ± 20 fs delay. The altered product branching ratio indicates that the presence of one solvent-like CO₂ molecule dramatically affects the electronic structure of the dissociating IBr⁻. We explore the origins of this phenomenon with classical trajectories, quantum wave packet studies, and MR-SO-CISD calculations of the six lowest-energy electronic states of IBr⁻ and 36 lowest-energy states of IBr. We find that the CO₂ molecule provides sufficient solvation energy to bring the initially excited state close in energy to a lower-lying state. The splitting between these states and the time at which the crossing takes place depend on the location of the solvating CO₂ molecule. © *2011 American Institute of Physics*. [doi:10.1063/1.3584203]

I. INTRODUCTION

One of the long-standing goals in chemistry is an in-depth understanding of reaction dynamics in solutions. Yet, a molecular-level view of chemistry requires significant experimental and computational effort, and investigations of state-resolved chemical dynamics in liquids remain a challenge.[1] In particular, chemical transformations that involve transitions among multiple electronic states are a subject of active interest due to their importance and diversity.[2–6] For example, multi-state dynamics determine the photostability of biological molecules,[4] underpin the activity of molecular switches,[5] and govern bimolecular reactions that include electronically excited species, such as chemiluminescence.[7] However, such dynamics are also intrinsically complex. Frequently, they involve strongly coupled atomic and electronic motions, leading to fast (sub-picosecond) redistribution of charge and vibrational energy within the reacting complex.[5] Since exact quantum-mechanical calculations of non-adiabatic dynamics are prohibitively expensive for all but the smallest systems, semiclassical methods are typically used.[3] Direct experimental investigations are also challenging because of the very fast timescales[8] and the broad, congested molecular spectra of the transient species. One fruitful experimental technique for disentangling the underlying dynamics of electronically excited polyatomic molecules is time-resolved photoelectron spectroscopy (TRPES).[5,9] Using femtosecond pump and probe laser pulses, TRPES has yielded exquisitely detailed pictures of non-Born-Oppenheimer processes, from small molecules[10,11] to DNA bases.[12]

The presence of solvent adds further complexity to chemical transformations and a detailed microscopic view of them must address explicitly both the intrinsic solute dynamics and the solute-solvent interactions. Solvent effects are especially pronounced in reactions of ionic or polar species,[7] and, in general, solute charge distributions are very sensitive to their environment. The influence of solvent on charge flow was explored by Bragg *et al.* in a recent investigation of atomic electron-transfer reactions in liquids.[13] An even more detailed view of solvent-mediated reactivity is afforded by gas-phase clusters with small numbers of solvent molecules. Specifically, ionic clusters[14,15] are attractive targets for TRPES because they are straightforward to size-select and provide access to well-characterized solvent environments. In several benchmark examples, partially solvated anions clustered with O₂, CO₂, or Ar exhibited behavior reminiscent of processes seen in bulk solvents, e.g., solvent-induced caging and energy relaxation.[16–19] Another recent study of NO⁺(H₂O)ₙ clusters showed that as few as four solvent molecules can profoundly affect the solute reactivity within small clusters,[20] highlighting the importance of solute-solvent interactions on a single-molecule scale. The experiments described here also take advantage of cluster anions to explore solvent-mediated charge transfer in dissociation reactions, one solvent molecule at a time.

---

a)Present address: Sandia National Laboratories, Livermore, California 94550, USA.
b)Present address: Department of Chemistry, Pennsylvania State University, University Park, Pennsylvania 16802, USA.
c)Present address: NASA Goddard Space Flight Center, Greenbelt, Maryland 20771, USA.
d)Authors to whom correspondence should be addressed. Electronic addresses: carl.lineberger@colorado.edu; mccoy@chemistry.ohio-state.edu; and rparson@jila.colorado.edu.
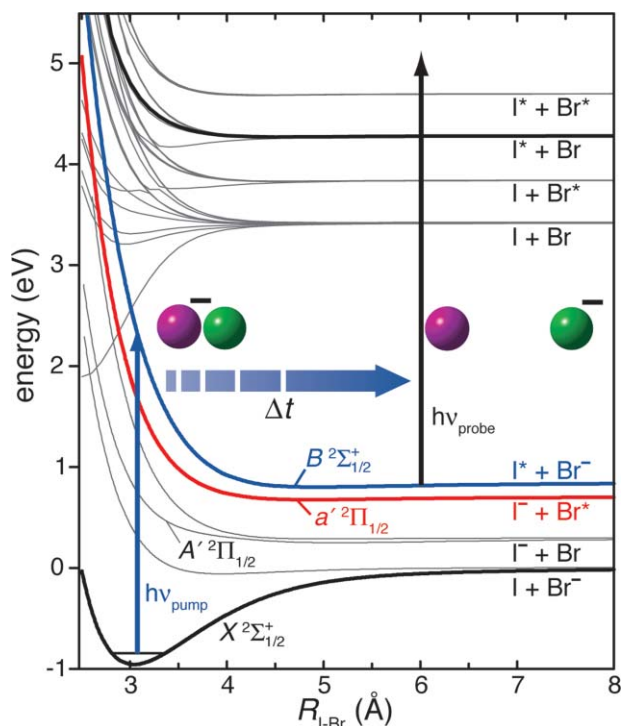
FIG. 1. The electronic states of IBr$^-$ and IBr, calculated at the MR-SO-CISD level of theory, and a cartoon of the experimental scheme. The vertical arrows $h\nu_{pump}$ and $h\nu_{probe}$ represent the pump and probe laser pulses, and the horizontal arrow Δt is the pump-probe delay time. The purple and green spheres are the I and Br atoms, respectively. The initial excitation is from the ground electronic state solely to the B state (blue curve); subsequent dissociation dynamics of IBr$^-$(CO$_2$) involve both the B state and the a' state (red curve). The bold black IBr potential energy curve shows the only electronic state of IBr that is accessible by one-electron probe photodetachment at $\Delta t = 0$.

We recently reported a combined experimental and theoretical investigation of charge transfer, mediated by a single solvent molecule, by using an IBr$^-$ anion clustered with just one CO$_2$ molecule.[21] That study focused on the dissociation of IBr$^-$ on the second excited (A') electronic state, which correlates adiabatically to I$^-$ + Br photoproducts (see Fig. 1 for a plot of the potential energy curves of IBr$^-$). Using a TRPES probe, we found that the presence of the CO$_2$ molecule enabled the excess electron to hop from the iodine to the bromine atom at a time delay of 350 fs following the electronic excitation of IBr$^-$(CO$_2$). Analysis of the potential energy curves indicated that this time delay corresponded to an I–Br separation of roughly 7 Å, slightly more than twice the equilibrium bond length of IBr$^-$ in its ground electronic state. Molecular dynamics (MD) simulations of this process showed that solvent motion modulated the electronic state energies of IBr$^-$. In the simulated complexes with favorable initial geometries, the A' state was brought into near-resonance with a lower-energy A state (which correlates to I + Br$^-$), thus facilitating non-adiabatic transitions. Yet, the energy gap between these two electronic states remained large over most of the potential energy surface sampled by the complexes, and as a result, only about 3% of IBr$^-$(CO$_2$) clusters underwent charge transfer.

Here we report a time-resolved investigation of dissociation dynamics in IBr$^-$ and IBr$^-$(CO$_2$), excited to the higher-lying B electronic state. The present experiment, inspired by

the results of our earlier study, further tests our theoretical model by probing solvent-driven electron transfer from a different electronic configuration. Unlike the A' state, the B state correlates to I* + Br$^-$ photoproducts,[22,23] and therefore the TRPES probe accesses a different set of neutral IBr electronic states. Under our experimental conditions, B-state photodissociation also yields a higher fragment translational energy release, leading to a faster and more energetic dissociation. Even more importantly, the asymptotic energy of the a' state, which correlates to charge-transferred I$^-$ + Br* products, is only 0.18 eV below that of the B state.[22,23] This is in contrast to our A' state study, where the nearest-neighbor charge-transfer A state was more than 0.3 eV lower in energy. Solvation energy of a single CO$_2$ molecule is $\sim$0.2 eV, sufficient to switch the energetic order of the B and a' states, but not of the A' and A states. This key difference is reflected by the experimental results: in the case of B-state photodissociation, addition of just one CO$_2$ molecule to IBr$^-$ induces abundant charge transfer.

II. EXPERIMENTAL METHODS

The experimental apparatus, described in greater detail previously,[22,24,25] combines a pulsed cluster anion source with a 100-fs laser system and a velocity-map imaging photoelectron spectrometer for TRPES measurements. The gas-phase cluster anion source[22] uses a pulsed General Valve nozzle to produce an expansion of neutral IBr seeded in 20 psi of CO$_2$ at 100 Hz. A focused beam of 1 keV electrons from an electron gun intersects the gas expansion and forms a range of cluster anions, which are then mass-separated in a Wiley-McLaren time-of-flight (TOF) spectrometer. The TOF region also contains electrostatic focusing optics and a fast potential switch that re-references the anions to earth ground.

The femtosecond laser system[25] is a Ti:Sapphire regenerative/multipass amplifier (Titan, Quantronix), seeded by 100-fs pulses from a Ti:Sapphire oscillator (Mira, Coherent). It operates at 400 Hz and produces pulses of 120 fs duration with a center wavelength of 788 nm, bandwidth of 10 nm, and energy of 3.3 mJ. The amplified output undergoes several non-linear mixing stages to form pump (500 μJ, 394 nm) and probe (30 μJ, tunable near-UV) laser pulses. Both beams are mildly focused and enter the photoelectron spectrometer collinearly. A computer-controlled mechanical positioning stage introduces a variable delay into the optical path of the pump pulse. The experimental temporal resolution, measured by a cross-correlation of the pump and probe pulses in a non-linear crystal, is 300 fs.

The velocity-map imaging photoelectron spectrometer[24] uses a three-element focusing lens, a 20-cm magnetically shielded field-free region, and an electron detector. The detector (Burle) is a pair of imaging-quality microchannel plates (MCPs) coupled to a phosphor screen and a CCD camera (LaVision), equipped with data acquisition software. The ion flight, laser propagation, and electron extraction axes are mutually perpendicular and intersect at the spatial focus of the spectrometer. Two high voltage switches supply pulsed imaging lens and MCP voltages for a brief "on" time, coincident with the arrival of the ion packet, to reduce back-

ground electron counts. The energy resolution of our spectrometer depends on the photoelectron kinetic energy, $\Delta E/E \approx 0.04$, or just a few milli-electron-volt for near-threshold electrons. However, the inherent bandwidth of femtosecond laser pulses limits the spectral resolution of TRPES experiments to ~30 meV or higher. In practice our instrumental resolution is 30–80 meV, sufficient to distinguish the photoproducts. The spectrometer energy scale is calibrated daily. The raw images are two-dimensional projections of the nascent photoelectron velocity vectors,[26,27] from which the full 3D velocity distributions are obtained with the basis set expansion (BASEX) algorithm.[28] Background signals due to detachment from ground-state anions by either the pump or probe pulse are removed by subtracting scaled 1-photon contributions (collected separately) from the pump-probe images. The difference images yield 2-photon pump-probe photoelectron spectra that arise solely from transient excited-state $I^{79}Br^-$ or $I^{79}Br^-(CO_2)$. The resulting spectra are reported in terms of the electron binding energy (eBE), which is the difference between the photon energy and the electron kinetic energy.

III. COMPUTATIONAL METHODS

A. Electronic structure calculations

Interpreting the dynamics in the TRPES experiment requires knowledge of the electronic states of IBr and IBr⁻ that involve excitations within the (σ, π, π^*, and σ^*) manifold of electronic states. The electronic structure calculations for IBr⁻ that are used in the present work were described previously.[21] Specifically, the electronic energies for the six lowest energy doublet electronic states of IBr⁻ and the 36 lowest energy states (21 singlet and 15 triplet) of IBr were calculated at the MRCI level of theory with singles and doubles, including spin-orbit coupling (MR-SO-CISD). We employed the pseudopotential, aug-cc-pVTZ-PP, from Peterson *et al.*[29,30] for I and Br. With these pseudopotentials iodine has a 28-electron core, and bromine has a 10-electron core. These pseudopotentials were chosen for their reliability and accuracy. All calculations were carried out using the MOLPRO suite of electronic structure codes.[31]

The calculations were carried out in three steps. First, state-averaged complete active space self-consistent field (CASSCF) calculations were performed using the C_{2v} point group. The active space consisted of all possible occupations of the six highest occupied molecular orbitals of IBr (σ, π, π^*, and σ^*) with 10 valence electrons for IBr and 11 valence electrons for the anion. All other occupied molecular orbitals were constrained to be doubly occupied. Consequently, the calculations on IBr and IBr⁻ included 21 singlet and 15 triplet states for the neutral and six doublet states for the anion, respectively. These were averaged with all states contributing equally to the averaging scheme. The orbitals from the CASSCF calculations were utilized in subsequent internally contracted MRCI calculations using the same sets of reference states. Spin-orbit coupling was then included via the state-interacting approach both at the CASSCF and MRCI levels of theory using the spin-orbit parameters of the pseudopotentials.

The resulting potential energy curves for the anion have been described previously.[21] In the case of neutral IBr, we analyzed the final eigenstates in terms of their zero-order contributions as well as the effective charges on the I and Br atoms. The charge distributions were approximated by taking the ratio of the dipole moment along the bond axis (in atomic units) to the IBr bond length (in Bohr). The resulting potential energy curves are plotted in Fig. 1. The only state of IBr that dissociates to I* + Br and that is expected to be accessible through a single electron loss channel near the ground state equilibrium configuration is highlighted in the plot. At larger I–Br separations, additional states will be accessible in the experiment. Since we do not know the relative cross-sections for electron loss via the states that correlate to I* + Br and the shapes of the curves are similar beyond 3.1 Å, we focus on the highlighted IBr state in the discussion that follows. The electronic energies of the six electronic states of IBr⁻ and the 66 neutral microstates as functions of the I–Br distance are provided in supporting material.[32]

B. Quantum dynamics

The approach used to model the photodissociation dynamics has been discussed previously,[33] and only relevant details will be reported here, with additional details provided in the supporting material.[32] We obtain the potential energy surfaces from the electronic structure calculations described above and use a sinc-discrete variable representation[34,35] to evaluate the nuclear states associated with the electronic states of IBr⁻ and IBr that are involved in the dynamics.

The approach used to model the experimental pump-probe dissociation process is based on the theoretical work of Batista *et al.* on the photodissociation of I_2^-,[36] and only the final equations will be given here. In the present study, the spectrum is modeled for a vibrational temperature of 200 K. Each of the thermally populated vibrational states on the ground electronic state is propagated on the *B* excited potential energy surface. Overlaps between the wave packet and eigenstates of the accessible neutral surface are then evaluated. For the reasons described above, we focus on the dynamics on the excited state of IBr that is highlighted in Fig. 1.

The expression for the time-resolved photoelectron signal, $P(\varepsilon, \Delta t)$, as a function of the electron kinetic energy (ε) and the pump-probe delay time (Δt), is given by

$$P(\varepsilon, \Delta t) = \hbar^{-4} \sum_n \left| \int_{-\infty}^{\infty} dt\, F_2(t - \Delta t) e^{[i/\hbar(E_n + \varepsilon - E_{\text{probe}})t]} \right.$$
$$\times \left[\sum_m c_m \langle \chi_n | \phi_m \rangle e^{[-i/\hbar(E_m)t]} \right.$$
$$\left. \left. \times \int_{-\infty}^{t} dt'\, F_1(t') e^{[i/\hbar(E_m - E_g - E_{\text{pump}})t']} \right] \right|^2 . \quad (1)$$

Here, $F_1(t')$ and $F_2(t-\Delta t)$ are the functional forms of the pump and probe pulses with characteristic energies E_{pump} (3.12782 eV) and E_{probe} (3.96749 eV), respectively. The

pulses have the following form:

$$F_j(t) = \mathrm{sech}^2 \left(\frac{t}{f \delta_j} \right), \tag{2}$$

where δ_j is the full width half maximum of the pulses and has values of 140 and 200 fs for the pump and probe pulses, respectively, and $\cosh[1/(2f)] = \sqrt{2}$. The subscripts n, m, and g in Eq. (1) represent the nuclear eigenstates of the accessed electronic state of neutral IBr and of the B and X electronic states of IBr$^-$, respectively, and $c_m = \langle \phi_m | \psi_g \rangle$. For the purpose of these calculations, the potential energy curves shown in Fig. 1 are used for I–Br distances between 1 and 48 a_0, and the potential is made to be infinite outside this region.

As a way to further understand the dissociation dynamics, particularly evolution on the B electronic state of IBr$^-$, we examine how the wave packet is dressed by the pump pulse and define the quantity,

$$\Xi_\mathrm{d}(R, \Delta t)$$

$$= \left| \sum_m c_m e^{[-i/\hbar(E_m)\Delta t]} \phi_m(R) \int_{-\infty}^{\Delta t} dt' F_1(t') e^{[i/\hbar(E_m - E_g - E_\mathrm{pump})t']} \right|^2. \tag{3}$$

$\Xi_\mathrm{d}(R, \Delta t)$ is the time-dependent probability amplitude on the B state, and its definition is simply the expression for $P(\varepsilon, \Delta t)$ when $F_2(t - \Delta t) = \delta(t - \Delta t)$ projected onto the I–Br distance coordinate, R. Additional details of these calculations are provided in the supporting material.[32]

C. Molecular dynamics simulations

The molecular dynamics simulations follow the approach reported in greater detail previously.[37,38] Briefly, the electronic structure of the solvated ion is given by an effective Hamiltonian on the basis of isolated IBr$^-$ electronic states within a classical perturbing field of the CO_2 solvent. The solute basis states are computed with the MOLPRO electronic structure package[39] at the MR-SO-CISD level of theory. The long-range electrostatic and polarization forces that dominate IBr$^-\cdots CO_2$ interactions are treated with special care by using distributed multipole expansions of the solute and solvent charge distribution.[40] The short-range dispersion and repulsion forces are represented by empirical pairwise atom-atom potentials.

For each ensemble of trajectories we compile 1000 starting cluster anion geometries by repeated sampling from a single trajectory on the ground electronic state at a temperature of 200 or 250 K. We then promote the trajectories to the B state, conserving their internal kinetic energy, and propagate them, diagonalizing the effective electronic Hamiltonian at each 1-fs time step. The simulations account for non-adiabatic transitions with a variant of the surface hopping algorithm of Hammes-Schiffer and Tully.[41,42] The trajectories are terminated when the distance between the iodine and bromine atoms exceeds 20 Å. Despite the limitations imposed by our use of a rigid, classical CO_2 molecule, this approach has been shown to adequately describe the molecular dynamics and charge flow within gas-phase cluster anions.[23,43]

IV. RESULTS AND DISCUSSION

A. Electronic structure calculations of IBr$^-$ and IBr

The calculated anion and neutral potential energy curves are plotted in Fig. 1. As mentioned above, the anion potentials were used in previous studies of IBr$^-$, while the neutral potential energy curves were obtained for the present study. The values of the energies and dipole moments for all 66 states, along with their symmetries within C_{2v}, are provided in the supporting material.[32] Asymptotically two singlet and two triplet states correlate to I* + Br and one singlet and one triplet state correlate to I* + Br*. However, based on the analysis of spin-orbit wavefunctions, only one of these states can be accessed by a single electron loss when IBr$^-$ is still near its X-state equilibrium I–Br distance. In the time-dependent calculations of the TRPES signal for IBr$^-$ on the B state, we only consider the detachment to the IBr electronic state that is plotted with the bold black line in Fig. 1.

B. Photodissociation of IBr$^-$

Experimental data for IBr$^-$ are relatively straightforward to interpret. The molecular orbital configuration of ground-state IBr$^-$ is $(\sigma)^2 (\pi)^4 (\pi^*)^4 (\sigma^*)^1$, abbreviated as 2441,[44] and the B-state configuration is 1442. Owing to its $\sigma^* \leftarrow \sigma$ character, the $B \leftarrow X$ electronic transition in IBr$^-$ is quite strong. The nearby a and a' electronic states are optically dark,[23] and thus in our experiments, the excitation is solely to the B state. Earlier experiments[45] have established that at the pump wavelength used here (394 nm) the only negatively charged photoproducts are Br$^-$, implying adiabatic dissociation on the B state.

Figure 2 presents experimental results for IBr$^-$ dissociation, collected using a probe wavelength of 313 nm ($E_{h\nu}$ = 3.96 eV). Panel 2(a) shows the transient photoelectron spectra, which reflect the evolution of the excited IBr$^-$ ensemble on the B state. These spectra are plotted versus electron binding energy, eBE = $E_{h\nu}$ – eKE, as a function of pump-probe delay. The false color scale in the corner of Fig. 2(a) indicates signal intensity. The spectra contain two well-separated peaks that grow in intensity and shift to slightly lower eBE between $\Delta t = 0$ and 0.5 ps, remaining essentially unchanged at longer delay times.

Panel 2(b) is a reference photoelectron spectrum of Br$^-$, mass-selected directly from the anion source under the same experimental conditions. The reference trace shows that both transient IBr$^-$ photoelectron peaks at $\Delta t > 0.5$ ps originate from probe detachment of Br$^-$ products (to form neutral Br and Br* at eBE = 3.36 and 3.82 eV, respectively).[46,47] The small spectral shift and otherwise overall similarity of the transient signal at $\Delta t < 0.5$ ps indicates that it arises from a region of the B-state potential energy surface where the excess charge has already localized on the Br atom. This observation agrees with other direct dissociation studies, which suggest that the atomic character of the products develops within the
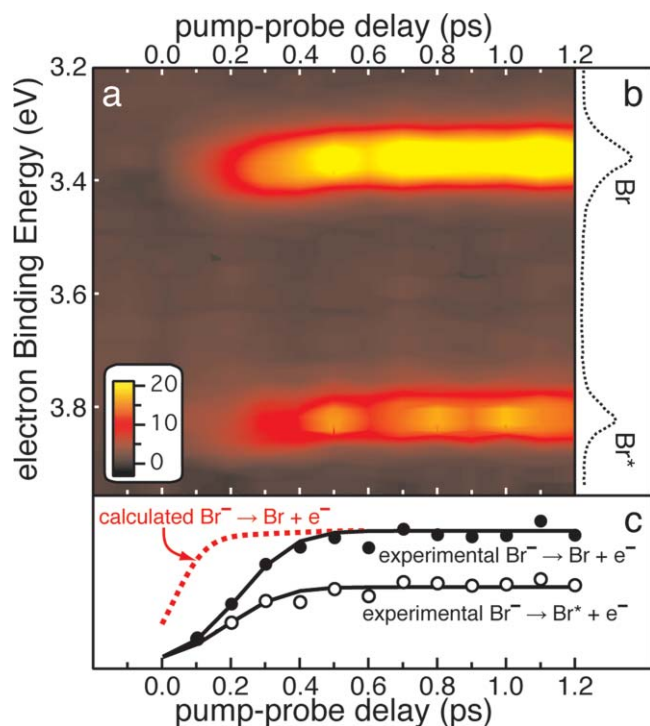
FIG. 2. Photodissociation of IBr⁻. Panel (a): Transient photoelectron spectra as a function of pump-probe delay time, Δt. The false color scale in the lower left hand corner indicates the relative intensity of the photoelectron signal. Panel (b): Reference photoelectron spectrum of Br⁻, showing transitions to the ground and spin-orbit excited states of neutral Br. Panel (c): The experimental and calculated signal intensity. Black and white circles are the integrated intensities of the Br and Br* photoelectron peaks. Solid black lines are least-squares fits of the data to the instrument response function convoluted with a step-function with a 200 ± 20 fs delay, as described in the text. Dotted red line is the integrated intensity of the Br peak in the calculated TRPES spectra.

first picosecond after electronic excitation.[48,49] To quantify the evolution of the experimental signal, we plot in Fig. 2(c) the integrated intensity of the two transient peaks as a function of pump-probe delay with circles. The black solid lines represent the least-squares fits of the peak intensities to an error-function form, $erf(\Delta t - t_{rise})$, under the assumption that the signal rise is very fast (step-like) and convoluted with our experimental resolution, 300 fs. The only adjustable fit parameter other than the arbitrary peak amplitude is the signal rise delay, $t_{rise} = 200 \pm 20$ fs. Evidently, B-state dissociation yields purely Br⁻, which enters our experimental detection range abruptly (compared to the experimental resolution) at $\Delta t = 200$ fs.

The time-resolved data presented in Fig. 2 are in line with earlier studies of IBr⁻ photolysis at $\lambda = 395$ nm and reveal prompt B-state dissociation to I* + Br⁻ products.[45] However, the transient signals in Fig. 2(c) also reveal a curious detail: at early times there is no detectable detachment from excited IBr⁻ in the molecular regime, and atomic-like Br⁻ products enter our detection range at $\Delta t = 200$ fs. In contrast, the rise curve of the integrated intensities obtained from the calculated transient photoelectron spectrum shows no such delay, as is represented by the dotted red line in Fig. 2(c).

Comparing the red and black lines in Fig. 2(c), we conclude that the delayed rise of the experimental signal is not

due to the energy difference between the B state of IBr⁻ and the electronic state of IBr accessed by probe photodetachment. Instead, the delayed rise likely reflects the changing photodetachment cross-section of transient IBr⁻ on the B state. The electronic character of the anion and neutral states evolves rapidly at short I–Br distances, i.e., in the "molecular" regime, yet we do not have the information needed to incorporate the internal coordinate dependence of the detachment cross-sections in the calculated spectra. We believe that this omission from the calculation is the source of the difference between the times of the rise, displayed by the black and red curves in Fig. 2(c). Interestingly, in the earlier study[33,48] of the TRPES obtained by first exciting IBr⁻ to the A' state followed by detachment, we found that both experiment and calculation displayed an instantaneous rise of the signal. Analysis of the calculated signal in that study showed that the intensity at short pump-probe delay times came primarily from two-photon direct detachment. If we assume that this channel for electron loss is closed on the B state, we can ask the questions, (1) at what I–Br distances has the system reached the asymptotic region of the potentials? and (2) if we set the detachment cross-section to zero at shorter distances and unity at longer distances, what would the rise curve look like?

To address these questions we perform two additional calculations. First, as plotted in Fig. 3(a), we calculate the charge on the iodine as a function of I–Br distance for all six electronic states of IBr⁻. In the case of the B state, the excess charge, which is slightly shifted toward iodine in the ground state equilibrium geometry of IBr⁻, smoothly localizes on bromine by a separation of ∼6 Å. In the second calculation, we obtain $\Xi_d(R, \Delta t)$, defined in Eq. (3), for various pump-probe delay times, which represents the probability amplitude on the B state obtained when the wave packet is dressed by the pump pulse. In Fig. 3(b) we plot the time-evolving wave packet that results from promotion of the $v = 0$ vibrational state of the anion. Finally, in the inset of Fig. 3(b), we evaluate the probability amplitudes associated with $R > 6$ Å, obtained from the cuts in Fig. 3(b). This analysis, which assumes that probe photodetachment from the B state is possible only after charge localization on the Br, leads to a delayed signal rise of approximately 160 fs. This value is very close to the experimentally observed value. This approach was previously employed by some of us to interpret the results of a time-resolved photodetachment (photoionization) study of the Cu–HOH system.[50,51]

C. Photodissociation of IBr⁻(CO₂)

IBr⁻(CO₂) clusters are bound by ∼0.2 eV and can be adequately described as IBr⁻ anions solvated by one CO₂ molecule.[23,24] The presence of this single solvent molecule drastically changes the product distribution following excitation of IBr⁻ to the B state. Figure 4(a) shows the transient photoelectron spectra as a function of pump-probe delay, and Fig. 4(b) is a composite reference photoelectron spectrum of Br⁻ and I⁻ anions. The transient spectra clearly reflect a mixed product distribution of Br⁻ and I⁻ as a result of at least two dissociation channels. Figure 4(c) shows the integrated
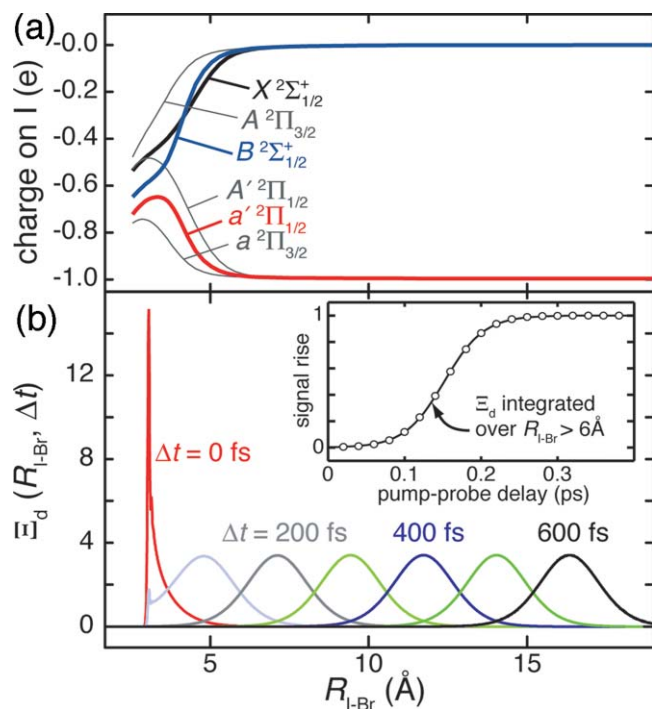
FIG. 3. Panel (a): Calculated charge of I in IBr$^-$ as a function of the I–Br distance. Panel (b): Quantum wave packet propagation results for IBr$^-$. $\Xi_d(R_{I-Br}, \Delta t)$ is the B-state probability amplitude arising from the $v = 0$ vibrational state of the anion prior to photodetachment. $\Xi_d(R_{I-Br}, \Delta t)$ is plotted at select values of Δt, from 0 to 600 fs. Inset: $\Xi_d(R_{I-Br}, \Delta t)$, integrated over I–Br distances where charge has localized on the Br atom ($R_{I-Br} > 6$ Å), as a function of Δt. The resulting curve approximates the experimental signal rise, assuming that probe photodetachment of transient B-state products becomes possible after excess charge localization.

intensities of the Br ← Br$^-$ and I ← I$^-$ transient peaks, which reflect the temporal evolution of the two product species. The Br$^-$ and I$^-$ products exhibit instrument-limited rise times, delayed by 250 ± 20 and 50 ± 20 fs, respectively.

Analysis of the experimental data leads us to two conclusions. First, in addition to dissociation on the initially excited state to form I* + Br$^-$, there now exists another product channel, most likely arising from a transition to a lower-lying electronic state that produces I$^-$ + Br*. The intense I$^-$ product peak, along with the prompt signal rise, indicates abundant electron transfer at short pump-probe delays and suggests crossing or near-avoided crossings of the B and a' states of IBr$^-$, driven by a single CO$_2$ molecule. The second conclusion, evident from Fig. 4(c), is that in the molecular regime (during the first 0.5 ps of dissociation) probe photodetachment is possible from I$^-$-based products at I–Br distances close to the ground-state equilibrium bond length of IBr$^-$. This contrasts with the Br$^-$-based products, where detachment is only observed for much larger I–Br distances. As a result, the Br$^-$-based and I$^-$-based transient signals appear in our spectra at delay times $\Delta t = 250$ and 50 fs, respectively. Notably, the Br$^-$-based signal delay, 250 fs, is very similar to the analogous delay in bare IBr$^-$, while the rise of the I$^-$-based signal is much faster.

The asymptotic photoproduct distribution in the dissociation of IBr$^-$(CO$_2$) is 60% Br$^-$ and 40% charge-transferred I$^-$, assuming approximately equal photodetachment cross-

sections for the two atomic products at our probe wavelength. It is also possible that photodissociation of IBr$^-$(CO$_2$) could form vibrationally excited cluster anion photoproducts, Br$^-$(CO$_2$) or I$^-$(CO$_2$). Such products would have distinct photoelectron spectra around eBE = 3.5 and 3.2 eV,[47,52] respectively. However, such products were not observed in the picosecond photofragmentation experiments,[45] which were sensitive to <1% cluster ion photofragment products. Our data are consistent with this earlier conclusion.

Our findings highlight two important differences from our previous study of IBr$^-$(CO$_2$) dissociation on the A' electronic state:[21] the much higher overall amount of electron transfer following excitation of IBr$^-$ to the B state and the absence of cluster anion products. The latter point is explained easily by the substantially higher kinetic energy release of B-state dissociation: 1.24 eV, compared to only 0.3 eV for the A' experiment. Yet, even in such a different energy regime, the solvent-mediated charge transfer model used in our earlier work successfully explains many of the present results and elucidates the reason for the abundant charge-transfer transitions.

Electronic structure calculations and the model that we use to study the classical dynamics both yield an equilibrium structure of the IBr$^-$(CO$_2$) complex in which the CO$_2$ molecule lies perpendicular to I–Br bond axis and is located near the center of the IBr bond. This is consistent with the observation that in its minimum energy geometry, the partial charges of the iodine and bromine atoms in IBr$^-$ are roughly equal, as shown in Fig. 3(a). This structure has been depicted
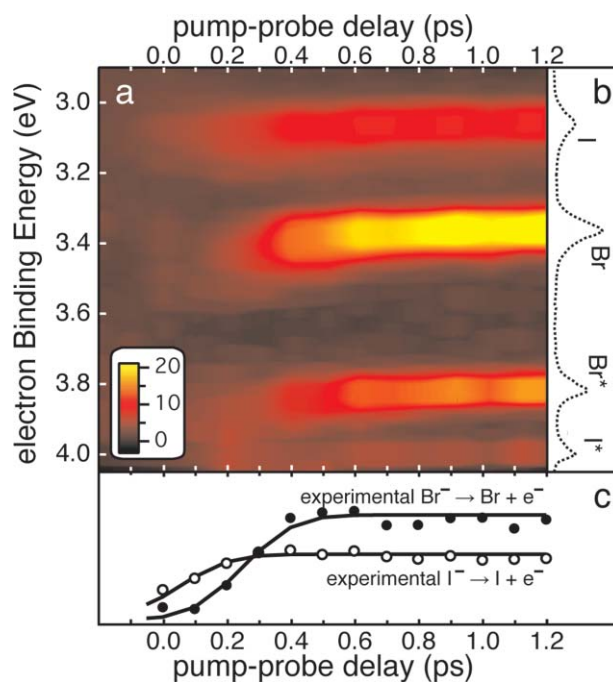

FIG. 4. Photodissociation of IBr$^-$(CO$_2$). Panel (a): Transient photoelectron spectra as a function of pump-probe delay time, Δt. Panel (b): Reference photoelectron spectra of I$^-$ and Br$^-$, showing transitions to the ground and spin-orbit excited states of neutral I and Br. Panel (c): The integrated intensity of the I (white circles) and Br (black circles) photoelectron peaks. The solid lines are least squares fits of the data, using instrument-limited rise times and appearance delays of 50 ± 20 fs (I peak) and 250 ± 20 fs (Br peak).
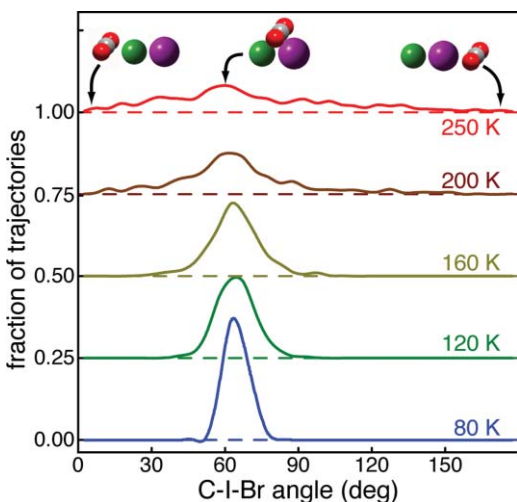
FIG. 5. The fraction of trajectories with specified C-I-Br angles is plotted for a range of temperatures. The corresponding geometries are depicted at the top of the figure. The ensembles at 200 and 250 K are used in the analysis of the excited state dynamics. The plots have been shifted by multiples of 0.25 to make it easier to see changes, and in all cases zero probability is indicated by the corresponding dashed line.

in the center of Fig. 5. As we increase the temperature of the cluster, the CO_2 molecule samples a wider range of orientations relative to IBr⁻. This is seen in the plots in Fig. 5. At the temperatures considered in the present study, 200 and 250 K, the CO_2 molecule is able to explore all orientations relative to the IBr⁻.

Electronic structure calculations of the excited states of IBr⁻ show that the negative charge, shared by I and Br at the ground-state equilibrium geometry, localizes rapidly on either the Br or I atom with increasing I–Br distance, as shown in Fig. 3(a). In particular, in the B state the charge becomes localized on the Br atom for distances larger than 3.5 Å, while in the a' state the charge localizes on the I atom. The introduction of a single CO_2 will stabilize the electronic states that have the excess charge near the CO_2 molecule while destabilizing others. For example, when the CO_2 molecule is near the Br atom, it brings the two states that correlate to the a' and B states in bare IBr⁻ closer in energy, leading, in some cases, to reordering of the energies of these states. Strictly speaking, the electronic states of the solvated anion cannot be uniquely identified by the state labels appropriate for the isolated solute,[38,43,53] so instead we characterize the electronic states by the atom on which the electron localizes at long times. Since this charge localization is much faster than solvent motion, the position of the CO_2 molecule prior to excitation will determine whether these states move closer together or farther apart in energy. Figure 6 illustrates this for two specific trajectories, while in Fig. 7 the correlation is illustrated for an ensemble of 1000 trajectories. In Fig. 6 we focus on the calculated properties of two MD trajectories, one in which the charge ultimately localizes on the iodine, forming I⁻ + Br*, and one that dissociates to form Br⁻ + I*. Both trajectories show that at early pump-probe delays, while the Br–C distance in Fig. 6(a) and 6(d) is small, the energy gap between the two states shown in Fig. 6(b) and 6(e) decreases from its value in bare IBr⁻. During this time, the evolution
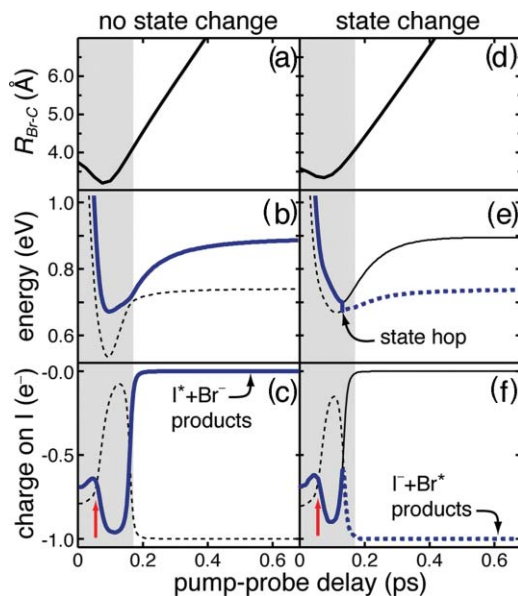

FIG. 6. Calculated properties of two representative MD trajectories at 200 K: one that dissociates to I* + Br⁻ photoproducts (a)–(c) and one that forms I⁻ + Br* (d)–(f). Panels (a) and (d): Distance between Br and C atoms, R_{Br-C}. Panels (b) and (e): Calculated electronic energies of IBr⁻(CO₂). Panels (c) and (f): Charge on the I atom. The solid and dotted lines in panels (b), (c), (e), and (f) designate the two states that are involved in the IBr⁻(CO₂) dynamics. The bold blue curve, which overlays one of the black lines, indicates the electronic state that determines the forces that control the classical dynamics. The shaded areas mark the time window before charge localization in bare IBr⁻ (about 160 fs). The red arrows in panels (c) and (f) mark the delay times for solvent-induced charge localization on the I atom (roughly 60 fs).

of the charge in Fig. 6(c) and 6(f) is also strongly perturbed from the expected behavior for the a' or B states in bare IBr⁻, as plotted in Fig. 3(a), and at delay times of roughly 60 fs the excess charge becomes localized on the iodine atom, as indicated by the red arrows. It is precisely this solvent-induced perturbation that enables both the state hop and the associated rapid reorganization of the solute charge distribution in the right-hand trajectory.
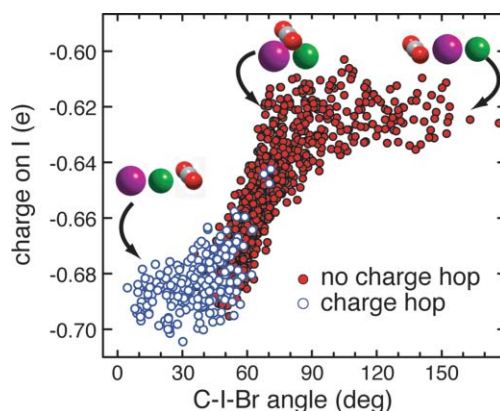

FIG. 7. Correlation between the initial IBr⁻(CO₂) geometry (represented by the C-I-Br angle), the initial charge on the iodine atom in IBr⁻ at $\Delta t = 10$ fs, and the likelihood of a charge hop event. Cartoons of the molecular geometry aid in visualizing the cluster configuration before photodetachment. Purple and green spheres represent I and Br atoms; gray and red spheres represent C and O atoms, respectively.
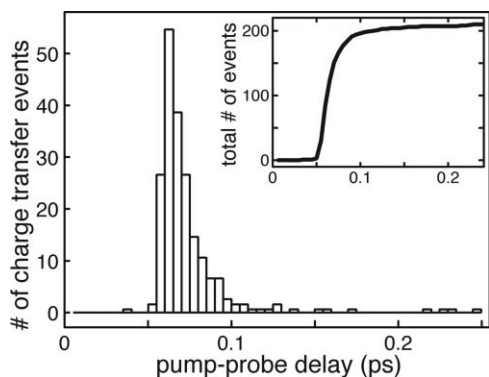
FIG. 8. Distribution of times at which excess charge localizes on I during photodissociation of $IBr^-(CO_2)$ at 200 K. Inset: total number of charge-transferred trajectories (out of 1000), as a function of pump-probe delay.

The larger number of charge-transferred photoproducts observed here stems from a crucial difference with respect to our earlier study of A'-state dissociation[21] of $IBr^-(CO_2)$: over much of the I–Br separation, the energy gap between the a' and B states in IBr^- is commensurate with the solvation energy of a single CO_2. Consequently, simulations of $IBr^-(CO_2)$ photodissociation predict that 22% of the trajectories asymptotically form $I^- + Br* + CO_2$ products at a vibrational temperature of 200 K, and 28% at 250 K. The difference between the 200 and 250 K ensembles reflects the correlation between charge transfer probability and initial cluster geometry, illustrated in Fig. 7. As seen in the plots in Fig. 5, these "warmer" cluster ensembles sample large ranges of initial geometries, and include configurations where CO_2 is located on the Br end of IBr^-. In this CO_2-Br-I geometry, corresponding to a C-I-Br angle of 0, the initially excited state is preferentially stabilized, bringing it closer, and in some cases lower, in energy than the state in which the charge has transferred from the bromine to the iodine atom. This leads to the non-adiabatic dynamics shown in the individual trajectories represented in Fig. 6.

The MD simulations correctly predict the timescale for solvent-induced localization of the excess charge on iodine. Figure 8 shows a histogram of the pump-probe delay times for transitions from the state that has more charge localized on the Br to the state that has more charge on the I. These times are also shown with red arrows in Fig. 6(c) and 6(f). The distribution of these times is quite narrow and peaks at $\Delta t = 60$ fs. This agrees with the experimentally observed rise of the I^- products and shows that the simulations capture the essential physics of charge flow in $IBr^-(CO_2)$. However, the MD simulations underestimate the experimentally measured amount of I^- products. We suspect that a significant contributor to this discrepancy is the use of rigid CO_2 molecules in the simulation model. Based on photoelectron studies of $I^-(CO_2)$ and $Br^-(CO_2)$ by Neumark and co-workers[47,52,54] and our own calculations,[21] as much as 20% of the CO_2 comes off with one or more quanta in the OCO bend upon electron detachment. This electronic to vibrational energy transfer means that the two states that are involved in the dynamics can be separated in energy by up to 0.16 eV (or the energy of two quanta in the OCO bend) and still accommodate this charge

transfer. The neglect of this mechanism along with the use of semiclassical surface hopping approaches led to undercounting of charge-transferred Br^- products in our earlier study of the A' state dynamics. In the present investigation, it very likely results in a similar undercounting of the trajectories in which the excess charge localizes on the I atom.

V. CONCLUSION

We report a comprehensive experimental and theoretical study of the sub-picosecond dissociation dynamics of IBr^- and $IBr^-(CO_2)$ on the repulsive B electronic state. The experimental data reveal a single product channel ($I^* + Br^-$) in bare IBr^- with a delayed rise of 200 ± 20 fs. The calculations of the TRPES signal for IBr^- do not reproduce this delayed rise, despite using methodologies that previously reproduced the experimental results following excitation to a lower-energy A' state.[33] This discrepancy between experiment and theory leads us to conclude that the experimentally observed delay reflects the dependence of the detachment cross-section from the B excited state of IBr^- rather than underlying features of the potential energy curves. The details of the coordinate dependence of the B-state detachment cross-section remain unresolved, and analysis of the electronic eigenstates of IBr^- and IBr does not provide a simple picture for the origin of this observation.

In the case of $IBr^-(CO_2)$, the introduction of a single CO_2 molecule results in 40% of the dissociation products coming from the charge-transferred $I^- + Br^*$ product channel. While the delay in the rise of the Br^--based signal is nearly identical to that observed for bare IBr^- (250 ± 20 fs), the I^--based dissociation process occurs with a delay time of only 50 ± 20 fs. To understand the origin of the abundant $I^- + Br^*$ photoproducts, we employ a solvent-mediated charge transfer model, developed to interpret earlier experiments[21] on the photodissociation dynamics of $IBr^-(CO_2)$. The large amount of excess energy dissipated in B-state dissociation presents a serious test for our theoretical framework. Although our model cannot fully explain the Br^--based signal delay, it successfully reproduces the other major findings of the present study. The success of the model in describing the short-time behavior in two different dynamical regimes is encouraging as we consider non-adiabatic processes in more complex systems.

[1]C. G. Elles and F. F. Crim, Annu. Rev. Phys. Chem. **57**, 273 (2006).
[2]L. J. Butler, Annu. Rev. Phys. Chem. **49**, 125 (1998).
[3]A. W. Jasper, S. Nangia, C. Y. Zhu, and D. G. Truhlar, Acc. Chem. Res. **39**, 101 (2006).

[4] C. T. Middleton, K. de La Harpe, C. Su, Y. K. Law, C. E. Crespo-Hernandez, and B. Kohler, Annu. Rev. Phys. Chem. **60**, 217 (2009).

[5] A. Stolow, Annu. Rev. Phys. Chem. **54**, 89 (2003).

[6] G. A. Worth and L. S. Cederbaum, Annu. Rev. Phys. Chem. **55**, 127 (2004).

[7] A. Fernandez-Ramos, J. A. Miller, S. J. Klippenstein, and D. G. Truhlar, Chem. Rev. **106**, 4518 (2006).

[8] A. H. Zewail, Angew. Chem., Int. Ed. Engl. **39**, 2586 (2000).

[9] A. Stolow, A. E. Bragg, and D. M. Neumark, Chem. Rev. **104**, 1719 (2004).

[10] V. Blanchet, M. Z. Zgierski, T. Seideman, and A. Stolow, Nature (London) **401**, 52 (1999).

[11] O. Gessner, A. M. D. Lee, J. P. Shaffer, H. Reisler, S. V. Levchenko, A. I. Krylov, J. G. Underwood, H. Shi, A. L. L. East, D. M. Wardlaw, E. T. Chrysostom, C. C. Hayden, and A. Stolow, Science **311**, 219 (2006).

[12] C. Z. Bisgaard, H. Satzger, S. Ullrich, and A. Stolow, ChemPhysChem **10**, 101 (2009).

[13] A. E. Bragg, M. C. Cavanagh, and B. J. Schwartz, Science **321**, 1817 (2008).

[14] D. M. Neumark, J. Chem. Phys. **125**, 132303 (2006).

[15] A. Sanov and W. C. Lineberger, Phys. Chem. Chem. Phys. **6**, 2018 (2004).

[16] A. V. Davis, R. Wester, A. E. Bragg, and D. M. Neumark, J. Chem. Phys. **117**, 4282 (2002).

[17] B. J. Greenblatt, M. T. Zanni, and D. M. Neumark, Science **276**, 1675 (1997).

[18] D. H. Paik, N. J. Kim, and A. H. Zewail, J. Chem. Phys. **118**, 6923 (2003).

[19] J. M. Papanikolas, V. Vorsa, M. E. Nadal, P. J. Campagnola, H. K. Buchenau, and W. C. Lineberger, J. Chem. Phys. **99**, 8733 (1993).

[20] R. A. Relph, T. L. Guasco, B. M. Elliott, M. Z. Kamrath, A. B. McCoy, R. P. Steele, D. P. Schofield, K. D. Jordan, A. A. Viggiano, E. E. Ferguson, and M. A. Johnson, Science **327**, 308 (2010).

[21] L. Sheps, E. M. Miller, S. Horvath, M. A. Thompson, R. Parson, A. B. McCoy, and W. C. Lineberger, Science **328**, 220 (2010).

[22] T. Sanford, S. Y. Han, M. A. Thompson, R. Parson, and W. C. Lineberger, J. Chem. Phys. **122**, 054307 (2005).

[23] M. A. Thompson, J. P. Martin, J. P. Darr, W. C. Lineberger, and R. Parson, J. Chem. Phys. **129**, 224304 (2008).

[24] L. Sheps, E. M. Miller, and W. C. Lineberger, J. Chem. Phys. **131**, 064304 (2009).

[25] M. S. Taylor, J. Barbera, C. P. Schulz, F. Muntean, A. B. McCoy, and W. C. Lineberger, J. Chem. Phys. **122**, 054310 (2005).

[26] D. W. Chandler and P. L. Houston, J. Chem. Phys. **87**, 1445 (1987).

[27] A. T. J. B. Eppink and D. H. Parker, Rev. Sci. Instrum. **68**, 3477 (1997).

[28] V. Dribinski, A. Ossadtchi, V. A. Mandelshtam, and H. Reisler, Rev. Sci. Instrum. **73**, 2634 (2002).

[29] K. A. Peterson, D. Figgen, E. Goll, H. Stoll, and M. Dolg, J. Chem. Phys. **119**, 11113 (2003).

[30] K. A. Peterson, B. C. Shepler, D. Figgen, and H. Stoll, J. Phys. Chem. A **110**, 13877 (2006).

[31] MOLPRO, a package of *ab initio* programs designed by H.-J. Werner and P. J. Knowles, version 2008.1, R. D. Amos, A. Bernhardsson, A. Berning, *et al.*

[32] See supplementary material at http://dx.doi.org/10.1063/1.3584203 for the calculated potential energy curves of IBr and IBr⁻.

[33] S. Horvath, R. M. Pitzer, and A. B. McCoy, J. Phys. Chem. A **114**, 11337 (2010).

[34] Z. Bacic and J. C. Light, Annu. Rev. Phys. Chem. **40**, 469 (1989).

[35] D. T. Colbert and W. H. Miller, J. Chem. Phys. **96**, 1982 (1992).

[36] V. S. Batista, M. T. Zanni, B. J. Greenblatt, D. M. Neumark, and W. H. Miller, J. Chem. Phys. **110**, 3736 (1999).

[37] J. Faeder, N. Delaney, P. E. Maslen, and R. Parson, Chem. Phys. **239**, 525 (1998).

[38] P. E. Maslen, J. Faeder, and R. Parson, Mol. Phys. **94**, 693 (1998).

[39] MOLPRO, a package of *ab initio* programs designed by H.-J. Werner and P. J. Knowles, version 2002.6, R. D. Amos, A. Bernhardsson, A. Berning, *et al.*

[40] A. J. Stone, *The Theory of Intermolecular Forces* (Clarendon, Oxford, 1996).

[41] S. Hammes-Schiffer and J. C. Tully, J. Chem. Phys. **101**, 4657 (1994).

[42] J. C. Tully, J. Chem. Phys. **93**, 1061 (1990).

[43] R. Parson, J. Faeder, and N. Delaney, J. Phys. Chem. A **104**, 9653 (2000).

[44] R. S. Mulliken, J. Chem. Phys. **55**, 288 (1971).

[45] T. Sanford, Ph.D. thesis, University of Colorado, 2004.

[46] T. Andersen, H. K. Haugen, and H. Hotop, J. Phys. Chem. Ref. Data **28**, 1511 (1999).

[47] D. W. Arnold, S. E. Bradforth, E. H. Kim, and D. M. Neumark, J. Chem. Phys. **102**, 3510 (1995).

[48] R. Mabbs, K. Pichugin, and A. Sanov, J. Chem. Phys. **122**, 174305 (2005).

[49] P. Wernet, M. Odelius, K. Godehusen, J. Gaudin, O. Schwarzkopf, and W. Eberhardt, Phys. Rev. Lett. **103**, 013001 (2009).

[50] F. Muntean, M. S. Taylor, A. B. McCoy, and W. C. Lineberger, J. Chem. Phys. **121**, 5676 (2004).

[51] M. S. Taylor, F. Muntean, W. C. Lineberger, and A. B. McCoy, J. Chem. Phys. **121**, 5688 (2004).

[52] D. W. Arnold, S. E. Bradforth, E. H. Kim, and D. M. Neumark, J. Chem. Phys. **102**, 3493 (1995).

[53] M. Thompson, Ph.D thesis, University of Colorado, 2007.

[54] D. W. Arnold, S. E. Bradforth, E. H. Kim, and D. M. Neumark, J. Chem. Phys. **97**, 9468 (1992).